

Wireless Channel Characterization From 2 to 28 GHz in an Outdoor Parking Lot

José-María Molina-García-Pardo , Lorenzo Rubio , *Senior Member, IEEE*, Maria-Teresa Martínez-Inglés ,
Esteban Egea-Lopez , Antonio Mateo-Aroca , Vicent M. Rodrigo Peñarrocha ,
and Juan Reig , *Senior Member, IEEE*

Abstract—This letter presents wideband measurements and simulations ranging from 2 to 28 GHz conducted in a parking lot, with and without cars. The measurements have been carried out considering a transmitter placed in an elevated position, with an omnidirectional antenna. The receivers have been distributed in the parking area also using omnidirectional antennas. Furthermore, the OPAL open-source ray launching tool has been used to simulate the different propagation mechanisms. The CI, FI, CIF, and ABC propagation models have been considered, showing a consistent behavior of the propagation path loss exponent with the frequency. The results suggest that the presence of cars has a minimal impact on the path loss along all frequencies.

Index Terms—Channel modeling, channel sounding, line of sight (LOS), millimeter wave (mmWave), parking lot, propagation.

I. INTRODUCTION

MILLIMETER WAVE (mmWave) frequencies for 5G and beyond have gained undoubtable attention as the mean of increasing allocating frequencies and bandwidth [1]. The availability of large bandwidths from 6 to 300 GHz in the spectrum is being used to increase the throughput in wireless communications [2]. The International Telecommunication Union (ITU) predicted that the trend of exponential growth will continue and, by 2030, the overall mobile data traffic will reach astonishingly 5 zettabytes (ZB) per month [3]. The World Radio Conference (WRC) established 5G frequency bands in the conference held in Geneva in 2015 [4] and at the conference held in Sharm el-Sheikh in 2019 [5], and it is expected to add new frequencies at the conference to be held at the end of 2023 in Dubai [6].

Manuscript received 20 December 2023; accepted 3 February 2024. Date of publication 8 February 2024; date of current version 7 May 2024. This work was supported in part by the Ministry of Education and Science, Spain under Grant PID2022-136869NB-C32, and in part by the MCIN/AEI/10.13039/501100011033/ through the I+D+i Projects under Grant PID2020-119173RB-C21 and Grant PID2020-112675RB-C41. (*Corresponding author: José-María Molina-García-Pardo.*)

José-María Molina-García-Pardo, Esteban Egea-Lopez, and Antonio Mateo-Aroca are with the Information Technologies and Communications Department, Universidad Politécnica de Cartagena, 30202 Cartagena, Spain (e-mail: jose-maria.molina@upct.es; esteban.egea@upct.es; antonio.mateo@upct.es).

Maria-Teresa Martínez-Inglés is with the Departamento de Ingeniería y Técnicas Aplicadas, University Center of Defense, San Javier Air Force Base, 30720 Cartagena, Spain (e-mail: mteresa.martinez@ud.upct.es).

Lorenzo Rubio, Vicent M. Rodrigo Peñarrocha, and Juan Reig are with the iTEAM Research Institute, Universitat Politècnica de València, 46022 Valencia, Spain (e-mail: lrubio@dcom.upv.es; vrodrigo@dcom.upv.es; jreig@dcom.upv.es).

Digital Object Identifier 10.1109/LAWP.2024.3363904

The gap between frequencies range 1 (FR1) and 2 (FR2) will be reduced by considering several bands around 7 GHz, which would lead to a more continuous use of the spectrum. Moreover, the first phase of European Union (EU) 2020 5G public-private partnership (PPP) initiative is investigating the 6–100 GHz frequencies, including mmWave frequencies, for 5G's ultrahigh data rate mobile broadband, among other applications. Then, a more comprehensive understanding of radio wave propagation is crucial to any further development of wireless networks.

Lot of studies have been performed from the sub-6 GHz to THz in outdoor environments [7], [8], [9], including many different scenarios, frequency bands, and applications. The ITU considers several reference scenarios for propagation and channel modeling, such as urban (very high-rise, high-rise, and low rise), suburban, residential, or rural. As a particular case of applications in 5G and beyond (B5G) are the open-air parking lots (found in USA/European shopping malls, entertainment centers, universities, or business parks). To the best of the authors' knowledge, little research has been done in the study of propagation in this kind of scenarios.

Only a few works related to this scenario can be found in literature. In [10], an investigation of the car reflection case study for a different number of the parking lot rows at 26-GHz frequency band is proposed. The measurement campaigns were conducted at the University Technology Malaysia (UTM), Kuala Lumpur, Malaysia, and used directional horn and omnidirectional antennas for the transmitter and receiver side, respectively. In [11], the same authors present the path loss models at 28 and 38 GHz in a parking lot environment which represents the multiend users for future 5G applications. In [12], empirical path loss models for wireless sensor networks (WSN) deployment in indoor and outdoor car parking lots were presented. In [13], the authors proposed a method to predict path loss in parking buildings.

The objective of this letter is to model both analytically and experimentally the wireless channel in an outdoor parking lot, where the transmitter is located in a high building illuminating the parking area with an omnidirectional antenna within an extensive bandwidths merging FR1 and FR2. Furthermore, the effect of the presence of cars is also considered by measuring the wireless channel in two different situations, i.e., full of cars and empty.

The rest of this letter is organized as follows. Section II describes the channel measurements. Section III briefly introduces the simulation aspects with OPAL. Path loss



Fig. 1. Top view of the measured scenario.



Fig. 2. Two photographs of the measured scenario: With cars (left) and without cars (right).

models are reviewed in Section IV. The results are presented and discussed in Section V. Finally, Section VI concludes this letter.

II. CHANNEL MEASUREMENTS

A. Propagation Scenario

The propagation scenario is an open parking lot situated in the campus of the Universidad Politécnica of Cartagena, Spain. It is surrounded by several historical military buildings now used as academic university facilities. Furthermore, a Roman amphitheater is in the west part of the parking. A top view of the measured scenario is depicted in Fig. 1. The transmitter (Tx) was placed on top of one of the buildings (red diamond in Fig. 1), having line of sight (LOS) in all cases. Then, the measurement campaigns were performed on two different days, one with the parking lot full of cars, while for the second the parking was nearly empty with only three cars. In Fig. 1, the orange circles represent the measurement points. Photos of both days can be seen in Fig. 2. The receiver (Rx) antenna height was 1.25 m, while the Tx antenna was 16.3 m from the ground.

B. Measurement Procedure and Setup

All measurements have been performed using a commercial vector network analyzer (VNA) (Rohde & Schwarz ZVA 10 MHz–67 GHz). To reach all locations an additional radio over fiber (RoF) link (EMCORE, Optiva OTS-2, 40 GHz [14]) has been used. The number of frequency points was 35 000, and the bandwidth of the intermediate frequency filter was 100 Hz. Ultrawideband omnidirectional antennas (STEATITE

Q-PAR ANTENNAS, 0.8–40 GHz [15]) have been used at the Tx and Rx, with vertical polarization and omnidirectional radiation pattern in the horizontal plane. The antenna patterns were measured in an anechoic chamber at 15 different frequencies between 1 and 38 GHz. The antenna gain ranges in frequency from -2.2 to 6.9 dBi and the 3 dB beamwidth from 20° to 140° .

III. OPAL

Simulations have been done with OPAL, a ray-tracing propagation simulator based on graphics processing units (GPUs), using the shooting and bouncing (SBR) method. This tool, whose main features and performance are described in [16], has already been applied for the simulation of the propagation waves in tunnels [17]. A 3-D model of the environment was generated, including a terrain elevation. The values of conductivity and relative permittivity of each building walls, mainly brick and concrete, are obtained from [18]. Cars are modeled as two different sized reflective boxes on top of each other. Up to 30 reflections were simulated as well as a single diffraction. Twenty-six million rays were generated, with a resolution of 0.05° in both azimuth and elevation, resulting in a density of approximately two million rays per steradian.

IV. PATH LOSS MODELS

In this section, we review four path loss models, i.e., the single-frequency floating-intercept (FI) model, the single-frequency close-in (CI) free-space reference-distance model, the multifrequency CI model with a frequency-dependent term (CIF) model, and the multifrequency alpha-beta-gamma (ABG) model.

The FI model is defined as [19]

$$PL^{FI}(d) = \beta + 10\alpha \log_{10}(d) + \chi_{\sigma}^{FI} \quad (1)$$

where $PL^{FI}(d)$ is the path loss, in dB, as a function of the Tx–Rx distance d , β is the floating intercept point or offset parameter, expressed in dB, that represents the free-space path loss at 1 m distance, α is the path loss exponent (PLE) that characterizes the dependence of the path loss on distance, and χ_{σ}^{FI} is the large-scale fading that can be modeled as a zero-mean Gaussian distributed random variable with standard deviation σ (in dB), also known as shadow factor (SF). The FI model is used in the WINNER II and the 3rd Generation Partnership Project (3GPP) [20], [21].

The CI model is defined as [22]

$$PL^{CI}(d) = FSPL(f, 1 \text{ m}) + 10n \log_{10}(d) + \chi_{\sigma}^{CI} \quad (2)$$

where $FSPL(f, 1 \text{ m})$ is the free-space path loss at carrier frequency f at 1 m distance, n represents the PLE, and χ_{σ}^{CI} is the SF.

The CIF model is defined as [23]

$$PL^{CIF}(f, d) = FSPL(f, 1 \text{ m}) + 10n \left(1 + b \left(\frac{f - f_0}{f_0} \right) \right) \log_{10}(d) + \chi_{\sigma}^{CIF} \quad (3)$$

where $PL^{CIF}(f, d)$ represents the path loss, in dB, over frequency and distance, n is the PLE, b represents the linear

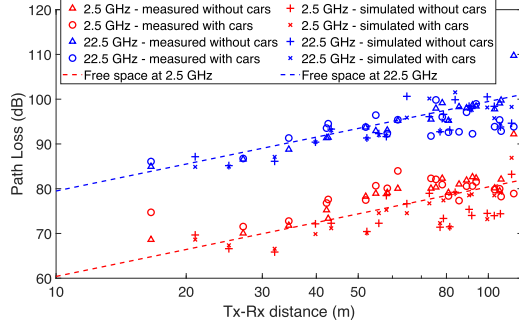


Fig. 3. Measured, simulated, and free-space path loss at 2.5 and 22.5 GHz, with and without cars.

frequency dependence of path loss on the weighted average of all frequencies, and f_0 is a reference frequency and it functions as a reference point for the linear frequency dependence of the PLE. The reference frequency f_0 is computed as $f_0 = (\sum_{k=1}^K f_k N_k) / \sum_{k=1}^K N_k$, where K is the number of frequency samples considered in the estimation of the model parameters, and N_k is the number of path loss data for the k th frequency f_k . The SF is characterized by the term χ_σ^{CIF} .

Finally, the ABG model is described as [24]

$$PL^{\text{ABG}}(f, d) = 10\alpha \log_{10} \left(\frac{d}{1 \text{ m}} \right) + \beta + 10\gamma \log_{10} \left(\frac{f}{1 \text{ GHz}} \right) + \chi_\sigma^{\text{ABG}} \quad (4)$$

where β is the floating intercept parameter, in dB, at 1 m of distance, α is the PLE, γ shows the dependence of path loss on frequency, f is the carrier frequency, expressed in GHz, and χ_σ^{ABG} is the SF to model the large-scale fading.

V. RESULTS

Due to the radiation pattern of the antennas and the noise floor of the VNA, a saturation effect can appear in the measured path loss, limiting the maximum Tx–Rx distance. To remove this effect, a preprocessing of the measurements has been done. The antenna gain effect has been corrected from the measured radiation pattern and has been also included in the simulation results. From the channel measurements, the path loss at the frequency f_0 is derived averaging the measured complex channel transfer function over a bandwidth of 1 GHz, as described in [25] and [26]. As an example, the measured and simulated path loss in terms of the Tx–Rx distance at 2.5 and 22.5 GHz, with and without cars in the parking lot, are depicted in Fig. 3. The free-space path loss has been included for comparison. Measured and simulation results are in good agreement, and no significant differences are observed to with and without cars propagation conditions.

From the path loss data, the parameters of the propagation models discussed in Section IV can be estimated by the least-squares linear fitting method using the `cftool` function of Matlab, as in [27]. The parameters of the FI model for the measured and simulated path loss are summarized in Tables I

TABLE I
PARAMETERS OF THE FI MODEL (MEASURED)

Freq.(GHz)	β (dB)	β^* (dB)	α	α^*	σ (dB)	σ^* (dB)
2.5	41.97	51.29	2.05	1.61	1.26	2.73
5.0	49.93	53.35	1.59	1.29	3.00	2.83
7.5	33.66	32.60	2.86	3.07	3.10	2.87
10.0	71.38	53.00	0.97	2.05	2.14	2.67
12.5	77.24	60.18	0.93	1.99	1.38	2.37
15.0	29.44	34.37	4.38	4.01	2.24	1.97
17.5	29.49	26.88	4.59	4.68	0.93	2.27
20.0	33.51	46.07	4.13	3.32	0.55	2.64
22.5	59.24	59.99	1.98	2.04	1.21	1.53
25.0	49.71	38.59	2.41	3.07	2.42	2.16
27.5	24.65	17.04	3.78	3.92	3.24	3.60

* indicates with cars.

TABLE II
PARAMETERS OF THE FI MODEL (SIMULATED)

Freq.(GHz)	β (dB)	β^* (dB)	α	α^*	σ (dB)	σ^* (dB)
2.5	50.75	45.47	1.27	1.57	3.00	1.90
5.0	32.42	39.80	2.49	2.01	3.78	0.93
7.5	55.15	52.77	1.53	1.65	3.75	2.06
10.0	46.73	45.55	2.23	2.30	4.16	1.06
12.5	53.94	49.70	1.90	2.16	2.17	1.30
15.0	50.78	45.35	2.22	2.59	2.57	1.92
17.5	53.31	57.59	2.12	1.87	1.18	0.60
20.0	62.33	56.82	1.64	2.11	1.57	2.62
22.5	59.83	58.32	1.90	1.97	2.83	1.41
25.0	50.99	51.85	2.49	2.46	2.24	1.34
27.5	61.15	64.31	1.98	1.77	2.91	1.57

* indicates with cars.

TABLE III
PARAMETERS OF THE CI MODEL (MEASURED)

Freq.(GHz)	$FSLP(f, 1 \text{ m})$ (dB)	n (dB)	n^*	σ (dB)	σ^* (dB)
2.5	40.40	2.13	2.28	1.23	2.84
5	46.42	1.79	1.71	3.57	3.34
10	52.44	2.04	2.09	3.06	2.49
12.5	54.38	2.30	2.34	3.03	2.31
15	55.96	2.66	2.65	3.68	3.07
17.5	57.30	2.74	2.75	3.27	4.09
20	58.46	2.47	2.53	2.88	2.81
22.5	59.48	1.96	2.07	1.14	1.40
25	60.40	1.75	1.73	2.57	3.21
27.5	61.22	1.62	1.20	5.34	6.08

* indicates with cars.

and II, respectively, with and without cars in the parking lot. For the measured path loss, the PLE adopts a mean value of 2.82 (with cars) and 2.70 (without cars), values that are higher than free-space propagation (PLE equal to 2). No correlation between the model parameters and frequency is observed. However, there is some correlation between the parameters β and α , as low values of α are associated with high values of β , and vice versa. This relationship between β and α was verified in [27] for vehicular-to-vehicular channel measurements. This behavior is explained by the fact that the FI model is based on a curve-fitting approach without any physical anchor [27]. From the simulated path loss, the mean PLE is 2.04 (with cars) and 1.98 (without cars), values very close to free-space propagation. It is important to note that at all Rx positions there is LOS condition.

Tables III and IV summarize the parameters of the CI model for the measured and simulated path loss, respectively. The mean PLE derived from the measured path loss is 2.14 (with cars) and 2.15 (without cars). From the simulated data, the mean value of

TABLE IV
PARAMETERS OF THE CI MODEL (SIMULATED)

Freq.(GHz)	$FSLP(f, 1 \text{ m})$ (dB)	n (dB)	n^*	σ (dB)	σ^* (dB)
2.5	40.40	1.85	1.88	3.14	1.86
5	46.42	1.71	1.61	4.00	1.12
7.5	49.94	1.82	1.82	3.68	1.95
10	52.44	1.91	1.88	4.08	1.23
12.5	54.38	1.88	1.89	2.06	1.31
15	55.96	1.89	1.91	2.35	2.06
17.5	57.30	1.85	1.89	1.08	0.55
20	58.46	1.90	2.00	1.40	2.40
22.5	59.48	1.93	1.89	2.68	1.29
25	60.40	1.91	1.94	2.32	1.54
27.5	61.22	1.98	1.96	2.77	1.51

* indicates with cars.

TABLE V
PARAMETERS OF THE CIF MODEL (MEASURED AND SIMULATED)

	b	b^*	n	n^*	σ (dB)	σ^* (dB)
Mea.	-0.0383	-0.1134	2.02	2.08	5.48	7.38
Sim.	0.0467	0.0622	1.87	1.88	3.20	1.95

* indicates with cars.

the PLE is 1.88 and 1.86 with and without cars, respectively. In both cases, the PLE values are very close, indicating that the path loss is independent of the presence or absence of cars in the parking lot. This indicates that the multipath effect caused by the presence of cars does not have a significant impact on the final In an analysis using OPAL, it has been found that by simulating random receivers within a circle of 1 m, the standard deviation is very similar with and without cars, being slightly higher with vehicles of the order of less than 1 dB. It is worth noting that the PLE values have a higher dispersion in terms of the frequency in the FI model, while they are more stable in the CI model due to the fact that term FSPL in (2) has an inherent frequency dependence of the path loss embedded for a distance equal to 1 m. With regard to the SF parameter, the lowest values are found for the simulated results and with the presence of cars in the parking, with major differences from the measured path loss when the FI and CI models are considered.

Comparing with literature, in [10], PLEs values of 2.6 and 4.6 were obtained for the CI and FI models, respectively, at 26 GHz when the Tx antenna is 2 m above the ground. Similarly, PLE values of 2.7 and 3.7 were reported in [11] for the CI model at 28 GHz also for 2 m Tx antenna height. These values of PLE are slightly higher since in our case the Tx antenna is in an elevated position.

The above models, do not take into account the dependence of path loss on frequency, and different values can be expected for each frequency. In order to have a complete model to describe the path loss variations in both distance and frequency, the CIF and ABG models include all measured path loss data, fitting the data in both domains, i.e., distance and frequency. As an example, the scatter plot of the measured path loss and the fitting results of both models are depicted in Fig. 4. Due to the log-scale in both distance and frequency axes, the measured path loss moves along a 2-D plane. Tables V and VI summarize the estimated model parameters for the CIF and ABG models, respectively. Based on the frequency samples considered, f_0 in the CIF model is equal

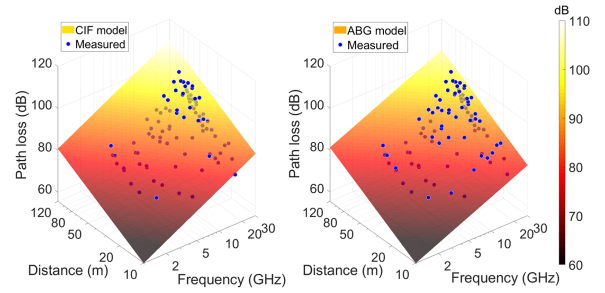


Fig. 4. CIF and ABG models from the measured path loss with cars.

TABLE VI
PARAMETERS OF THE ABG MODEL (MEASURED AND SIMULATED)

	α (dB)	α^* (dB)	β	β^*	γ	γ^*	σ (dB)	σ^* (dB)
Mea.	1.65	2.38	40.68	31.58	1.82	1.63	5.49	7.62
Sim.	1.95	2.01	28.32	26.99	2.27	2.29	3.24	2.01

* indicates with cars.

to 12.93 GHz for the measured data, and equal to 14.67 GHz for the simulated data. For the measured path loss, the mean PLE in the CIF model is close to 2, 2.08 with cars and 2.02 without cars, in accordance with the mean PLE derived for the CI model. Nevertheless, the path loss variability in presence of cars is higher, increasing the SF from 5.48 dB (without cars) to 7.48 dB (with cars). In the case of the ABG model the values of the SF are similar to the CIF model, showing a similar fitting error. However, the differences are larger for the PLEs. From the simulated path loss, the SF derived in both models is lower, and the PLE values are very close to the mean PLE values derived in the CIF and ABG models, showing that both models can describe the path loss in both distance and frequency, as an extension of the single frequency FI and CI models.

VI. CONCLUSION

Measurements in an open parking lot with the Tx antenna placed in an elevated position have been presented. A wide frequency range was measured, from 1 to 28 GHz. The path loss has been characterized through the single frequency FI and CI models, and the multifrequency CIF and ABG models. The results show that while the FI model minimizes the SF, the CI model gives a better physical behavior of the PLE, with values close to the free-space propagation. Similar mean values of the PLE have been derived from the measured path loss, 2.14 and 2.15 with and without cars, respectively. From the simulated path loss the values are slightly lower, with mean values of 1.88 and 1.86 with and without cars, respectively. The parameters derived for the multifrequency models allow us to describe the dependence of the path loss on both distance and frequency, with a PLE close to the mean values derived for the single frequency models. From the measured results, no major differences were found in the model parameters related to the presence or absence of cars in the parking.

Although the link budget is high at mmWave frequencies in this type of environment, being of the order of 95 dB and up to 100 m, the results suggest that it is possible to use omnidirectional antennas in the deployment of wireless communications.

REFERENCES

- [1] I. F. Akyildiz, A. Kak, and S. Nie, "6G and beyond: The future of wireless communications systems," *IEEE Access*, vol. 8, pp. 113995–134030, 2020.
- [2] M. Shafi et al., "Microwave vs. millimeter-wave propagation channels: Key differences and impact on 5G cellular systems," *IEEE Commun. Mag.*, vol. 56, no. 12, pp. 14–20, Dec. 2018.
- [3] "Cisco Annual Internet Report, "(2018–2023) White Paper," Cisco, San Jose, CA, USA, White Paper, 2020. [Online]. Available: <https://www.cisco.com/c/en/us/solutions/collateral/executive-perspectives/annual-internet-report/white-paper-c11-741490.html>
- [4] World Radiocommunications Conference 2015 (WRC-15), "Geneva, Switzerland, 2-27 November," 2015.
- [5] World Radiocommunications Conference 2019 (WRC-19), "Sharm el-Sheikh, Egypt, 28 October to 22 November," 2019.
- [6] World Radiocommunications Conference 2023 (WRC-23), "Dubai, United Arab Emirates, from 20 November to 15 December," 2023.
- [7] T. S. Rappaport et al., "Millimeter wave mobile communications for 5G cellular: It will work!," *IEEE Access*, vol. 1, pp. 335–349, 2013.
- [8] K. Haneda, "Channel models and beamforming at millimeter-wave frequency bands," *IEICE Trans. Commun.*, vol. E 98-B, no. 5, pp. 755–772, 2015.
- [9] Y. Xing and T. S. Rappaport, "Millimeter wave and terahertz urban microcell propagation measurements and models," *IEEE Commun. Lett.*, vol. 25, no. 12, pp. 3755–3759, Dec. 2021.
- [10] M. N. Hindia, A. M. Al-Samman, and T. Bin Abd Rahman, "Investigation of large-scale propagation for outdoor-parking lot environment for 5G wireless communications," in *Proc. IEEE 3rd Int. Symp. Telecommun. Technol.*, 2016, pp. 14–18.
- [11] A. M. Al-Samma, T. A. Rahman, M. N. Hindia, A. Daho, and E. Hanafi, "Path loss model for outdoor parking environments at 28 GHz and 38 GHz for 5G wireless networks," *Symmetry*, vol. 10, no. 12, 2018, Art. no. 672.
- [12] T. O. Olasupo, C. E. Otero, L. D. Otero, K. O. Olasupo, and I. Kostanic, "Path loss models for low-power, low-data rate sensor nodes for smart car parking systems," *IEEE Trans. Intell. Transp. Syst.*, vol. 19, no. 6, pp. 1774–1783, Jun. 2018.
- [13] S. Phaiboon, "Propagation path loss models for parking buildings," in *Proc. 5th Int. Conf. Inf. Commun. Signal Process.*, 2005, pp. 1348–1351.
- [14] "Optiva OTS-2 series microwave band 50 MHz to 60 GHz fiber optic links," Emcore, Alhambra, CA, USA, 2020. [Online]. Available: <http://emcore.com/products/optiva-ots-2-series-microwave-band-50-mhz-to-40-ghz-fiber-optic-links>
- [15] "Ultra-wideband omni-directional antenna 0.8 to 40 GHz," Steatite Antennas, Leominster, U.K., Catalogue no. QOM-SL-0.8-40-K-SG-L. [Online]. Available: <https://www.steatite-antennas.co.uk/wp-content/uploads/2017/09/QOM-SL-0.8-40-K-SG-L.pdf>
- [16] E. Egea-Lopez, J.-M. Molina-Garcia-Pardo, L. Lienard, and P. Degauque, "Opal: An open source ray-tracing propagation simulator for electromagnetic characterization," *PLoS ONE*, vol. 16, no. 11, 2021, Art. no. e0260060.
- [17] E. Egea-Lopez, J.-M. Molina-Garcia-Pardo, M. Lienard, and P. Degauque, "Deterministic polarimetric propagation analysis in road tunnels," in *Proc. Int. Wireless Commun. Mobile Comput.*, 2022, pp. 743–747.
- [18] *Effects of Building Materials and Structures on Radiowave Propagation Above About 100 MHz*, Recommendation ITU-R P.2040-1, 2015.
- [19] A. Zajic, *Mobile-to-Mobile Wireless Channels*. Norwood, MA, USA: Artech House, 2013.
- [20] "Spatial channel model for multiple input multiple output (MIMO) simulations," 3GPP, Paris, France, 3GPP TR 25.996, Sep. 2012.
- [21] P. Kyosti et al., "Winner II channel models," European Commission, IST-4-027756-WINNER, Tech. Rep. Tech. Rep. D1.1.2, 2007.
- [22] T. Rappaport, *Wireless Communications: Principles and Practice*, 2nd ed. Englewood Cliffs, NJ, USA: Prentice-Hall, 2001.
- [23] G. R. Maccartney, T. S. Rappaport, S. Sun, and S. Deng, "Indoor office wideband millimeter-wave propagation measurements and channel models at 28 and 73 GHz for ultra-dense 5G wireless networks," *IEEE Access*, vol. 3, pp. 2388–2424, 2015.
- [24] S. Piersanti, L. A. Annoni, and D. Cassioli, "Millimeter waves channel measurements and path loss models," in *Proc. IEEE Int. Conf. Commun.*, 2012, pp. 4552–4556.
- [25] L. Rubio et al., "Contribution to the channel path loss and time-dispersion characterization in an office environment at 26 GHz," *Electronics*, vol. 8, no. 11, 2019, Art. no. 1261.
- [26] L. Rubio et al., "Millimeter wave channel measurements in an intra-wagon environment," *IEEE Trans. Veh. Technol.*, vol. 68, no. 12, pp. 12427–12431, Dec. 2019.
- [27] L. Rubio et al., "Millimeter-wave channel measurements and path loss characterization in a typical indoor office environment," *Electronics*, vol. 12, no. 4, 2023, Art. no. 844.